ARTICLE

Deciphering synergetic core-shell transformation from [Mo_6O_{22}@Ag_{44}] to [Mo_8O_{28}@Ag_{50}]

Zhi Wang [1], Hai-Feng Su[2], Chen-Ho Tung[1], Di Sun [1] & Lan-Sun Zheng[2]

The structural transformation of high-nuclearity silver clusters from one to another induced by specific stimuli is of scientific significance in terms of both cluster synthesis and reactivity. Herein, we report two silver-thiolate clusters, [Mo_6O_{22}@Ag_{44}] and [Mo_8O_{28}@Ag_{50}], which are templated by isopolymolybdates inside and covered by $^iPrS^-$ and $PhCOO^-$ ligands on the surfaces. Amazingly, the [Mo_8O_{28}@Ag_{50}] can be transformed from [Mo_6O_{22}@Ag_{44}] by adding PhCOOH which increases the degree of condensation of molybdates template from $Mo_6O_{22}^{8-}$ to $Mo_8O_{28}^{8-}$, then enlarging the outer silver shell from Ag_{44} to Ag_{50}. The evolution of solution species revealed by time-dependent electrospray ionization mass spectrometry (ESI-MS) suggests a breakage-growth-reassembly (BGR) transformation mechanism. These results not only provide a combined assembly strategy (anion-template + induced transformation) for the synthesis of silver-thiolate clusters but also help us to better understand the complex transformation process underpinning the assembly system.

[1] Key Laboratory of the Colloid and Interface Chemistry, Ministry of Education, School of Chemistry and Chemical Engineering, Shandong University, 250100 Jinan, China. [2] State Key Laboratory for Physical Chemistry of Solid Surfaces, Department of Chemistry, College of Chemistry and Chemical Engineering, Xiamen University, 361005 Xiamen, China. These authors contributed equally: Zhi Wang, Hai-Feng Su. Correspondence and requests for materials should be addressed to D.S. (email: dsun@sdu.edu.cn)

With regard to their ubiquitous argentophilicity and variable coordination fashions[1–3], Ag(I) coordination complexes, especially for silver clusters, are gorgeous in structural diversity and physicochemical properties[4–6]. However, the synthesis of high-nuclearity silver clusters is always tedious and frankly a trial-and-error process. Overwhelming these synthesis barriers has promoted the appearance of exquisite assembly strategies including anion templation and geometric polyhedral principle[7,8], which have pushed the assembly of silver clusters to a higher level of sophistication[9,10]. From the known largest silver(I) solid cluster (Ag$_{490}$)[11] to the largest silver(I) cage (Ag$_{180}$)[12], we have witnessed the fruitful advances in this field. However, there is still vast room for improvement to realize the manipulation over such clusters at the molecular level, not just synthesizing them randomly. Inspired by the LEIST (ligand-exchange-induced size/structure transformation) methodology widely used in Au$_n$(SR)$_m$ nanoclusters[6], we would like to study whether the similar stories can be observed in their silver cousins. In 2012, Mak et. al., reported the reaction of a famous Cl@Ag$_{14}$ cluster with AgClO$_4$, which gave a larger Cl$_6$Ag$_6$@Ag$_{30}$ cluster, thus realizing the cluster enlargement[13]. Following this, a polyoxovanadate-templated Ag$_{30}$ cluster was subjected to acid/base stimulations, which only resulted in the reversible conversion of configurations of [V$^V_{10}$V$^{IV}_2$O$_{34}$]$^{10-}$ from D_{3d} to C_{2h}, however, the silver shell was kept invariable[14]. These sporadic reports indicated the structural transformation of silver clusters inside and out by specific stimuli is still a challenging task.

In order to achieve structural transformation of silver clusters, two prerequisites are needed: (i) flexible silver shells and (ii) variable anion templates. Installing monocarboxylate ligands on the surface of silver clusters will endow the silver clusters some flexibility because the carboxylate belongs to hard base with respect to thiolate, thus forming relatively weak bonding with soft acid Ag(I) atoms[15]. As such, when the stimuli-induced post-reaction proceeds in solution, the carboxylates can partially disassociate then induce the rearrangement of surface silver atoms. For variable anion templates, polyoxometalates (POMs) are the best candidates due to their mutable forms depending on pH values[16].

With all above considerations in mind, herein we use thiol and benzoic acid as mixed ligands to construct a silver cluster, [Mo$_6$O$_{22}$@Ag$_{44}$(^{i}PrS)$_{20}$(PhCOO)$_{16}$(CH$_3$CN)$_2$]·2CH$_3$CN (**SD/Ag44; SD = SunDi**), which can be transformed to another larger silver cluster, [Mo$_8$O$_{28}$@Ag$_{50}$(^{i}PrS)$_{24}$(PhCOO)$_{18}$(CH$_3$CN)$_2$)]·4CH$_3$CN (**SD/Ag50**) by the reaction with additional PhCOOH. To the best of our knowledge, this is the first report of the PhCOOH-induced structural transformation simultaneously involving enlargements of inner anion template (Mo$_6$O$_{22}^{8-}$ → Mo$_8$O$_{28}^{8-}$) and outer silver shell (Ag$_{44}$ → Ag$_{50}$). Such transformation is also proved by the time-dependent ESI-MS of **SD/Ag44** after adding PhCOOH and a breakage-growth-reassembly (BGR) mechanism is also proposed.

Results

Structures of SD/Ag44 and SD/Ag50. The **SD/Ag44** was synthesized by solvothermal reaction of polymeric (^{i}PrSAg)$_n$ precursor, PhCOOAg and (^{n}Bu$_4$N)$_4$(α-Mo$_8$O$_{26}$) in CH$_3$CN at 65 °C (Fig. 1). After the reaction, the yellow tufted crystals can be collected as the bulk sample of **SD/Ag44**. If adding another portion of PhCOOH (0.32 mmol) into above reaction mother liquor without removing crystals of **SD/Ag44**, then continuing to react again under the same condition will produce yellow block crystals of **SD/Ag50**.

The molecular structures of **SD/Ag44** and **SD/Ag50** were determined by single-crystal X-ray diffraction (SCXRD) analysis

(Supplementary Table 1). Both of them crystallize in triclinic P-1 space group with a complete cluster in the asymmetric unit. As shown in Fig. 2a, the overall structure of **SD/Ag44** is a slightly squashed spheroid composed of 44 silver atoms and covered by 20 ^{i}PrS$^-$, 16 PhCOO$^-$ ligands and two CH$_3$CN molecules. Interiorly, an unusual Mo$_6$O$_{22}^{8-}$ anion in situ generated from (^{n}Bu$_4$N)$_4$(α-Mo$_8$O$_{26}$) supports the outer Ag$_{44}$ shell. The diameter of **SD/Ag44** is roughly 1.2 nm, if removing the organic shell. Based on their coordination modes, 20 ^{i}PrS$^-$ ligands are divided into two types comprised of 2 μ$_3$ and 18 μ$_4$ (Fig. 2b), which capped on the irregular silver trigons, tetragons or pentagons with the Ag-S bond lengths spanning from 2.3641(17) to 2.7589(18) Å. The PhCOO$^-$ ligands with μ$_2$-κ^1:κ^1, μ$_3$-κ^1:κ^2, μ$_4$-κ^2:κ^2, and μ$_4$-κ^1:κ^3 modes cap on the edges or faces of silver polygons (Supplementary Fig. 2). The Ag-O$_{benzoate}$ bond lengths locate in the range of 2.114(5)−2.787(7) Å. Two additional CH$_3$CN molecules finally finish the coverage of Ag$_{44}$ shell (Ag-N: 2.338(7) and 2.395(6) Å), which is further consolidated by the Ag···Ag interactions (2.8272(7)−3.4289(8) Å)[17,18].
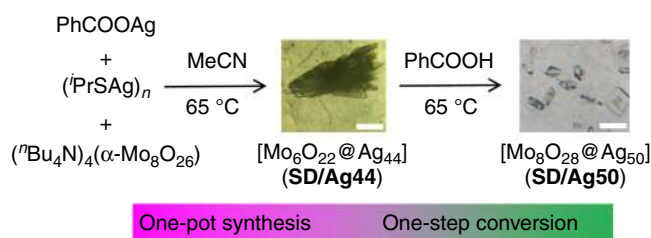

PhCOOAg + (^{i}PrSAg)$_n$ + (^{n}Bu$_4$N)$_4$(α-Mo$_8$O$_{26}$) →[MeCN, 65 °C] [Mo$_6$O$_{22}$@Ag$_{44}$] (**SD/Ag44**) →[PhCOOH, 65 °C] [Mo$_8$O$_{28}$@Ag$_{50}$] (**SD/Ag50**)

One-pot synthesis   One-step conversion

Fig. 1 Synthesis and transformation routes for **SD/Ag44** and **SD/Ag50**. The scale bar is 1 mm
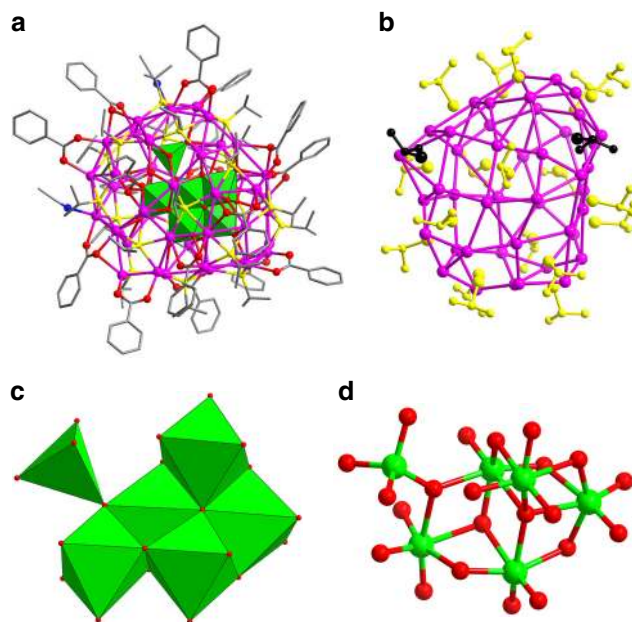

Fig. 2 Single-crystal X-ray structure of **SD/Ag44**. **a** The molecular structure of **SD/Ag44**. The inner POM anion template is shown in polyhedral mode (Color legend: Ag: purple; S: yellow; Mo: green; O: red; C: gray; N: blue). **b** The distributions of ^{i}PrS$^-$ ligands on the Ag$_{44}$ shell sorted by different coordination modes individually colored. Black: μ$_3$ and yellow: μ$_4$. The polyhedral (**c**) and ball-and-stick (**d**) modes showing the inner Mo$_6$O$_{22}^{8-}$ anion

Notably, a $Mo_6O_{22}^{8-}$ anion was trapped into the Ag_{44} cluster and should be in situ transformed from α-$Mo_8O_{26}^{4-}$. Bond-valence sum (BVS) calculations for six Mo atoms were performed and confirmed all of them are + 6 oxidation state (Mo1-Mo6: 5.744, 5.455, 5.792, 5.531, 5.766, and 6.173)[19]. This indicates that no redox reaction occurs under the reaction condition. The $Mo_6O_{22}^{8-}$ in **SD/Ag44** is constructed from five edge-shared MoO_6 octahedra adding one MoO_4 tetrahedron by sharing one vertex (Fig. 2c). Alternatively, it can be seen as three Mo_3O_4 opened cubanes fused together by sharing two Mo_2O_2 rhombus faces with another vertex-shared MoO_4 outside (Fig. 2d). This $Mo_6O_{22}^{8-}$ has 14 terminal O atoms, 5 μ_2 bridging O atoms and 3 μ_3 bridging O atoms. The Mo-O bond distances are in the range of 1.730(5)−2.328(4) Å, suggesting unusual elongated characteristic of Mo-O bonds compared to other $Mo_6O_{22}^{8-}$ anions in classic POM chemistry[20]. Using the μ_1 and μ_2 bridging O atoms, $Mo_6O_{22}^{8-}$ binds total 30 Ag atoms around it with the Ag-O_{POM} bond lengths ranging from 2.255(4) to 2.793(5) Å (Supplementary Fig. 3). To date, only three isomeric $Mo_6O_{22}^{8-}$ anion templates have been reported in silver clusters such as face-shared Mo_4O_4 double cubanes[21,22], two Mo_3O_4 opened cubanes sandwiching a Mo_4O_4 cubane by face-sharing[23], and three face-shared Mo_3O_4 opened cubanes[24], as summarized in Supplementary Table 2. By comparisons, the $Mo_6O_{22}^{8-}$ in **SD/Ag44** is the fourth isomer trapped by silver cluster. Moreover, such $Mo_6O_{22}^{8-}$ is also different from those observed in POM-based inorganic–organic hybrids (Supplementary Table 3)[25–27], suggesting a new $Mo_6O_{22}^{8-}$ structure.

When adding another portion of PhCOOH to the mixture after the synthesis of **SD/Ag44** for second step reaction, we can isolate a larger silver cluster, **SD/Ag50**. SCXRD analysis revealed that it is a larger cluster than **SD/Ag44**. The overall structure of **SD/ Ag50** comprised of 50 Ag atoms, forming a nearly ball-like shape with a diameter of *ca.* 1.4 nm, which is co-protected by 24 $^iPrS^-$, 18 $PhCOO^-$ ligands, and two CH_3CN molecules (Fig. 3a). The ratio of $^iPrS/PhCOO$ in **SD/Ag50** (4:3) is slightly larger than that in **SD/Ag44** (5:4), indicating the re-organization of two kinds of ligands on the surface after structural transformation. As shown

in Fig. 3b, 24 $^iPrS^-$ ligands show μ_4 and μ_5 binding modes, whereas $PhCOO^-$ ligands show μ_2-κ^1:κ^1, μ_3-κ^1:κ^2, μ_4-κ^1:κ^3, or μ_4-κ^2:κ^2 modes. The Ag-S and Ag-$O_{benzoate}$ bond lengths fall in the ranges of 2.248(7)−2.917(4) and 2.238(13)−2.771(12) Å, respectively. Due to the lack of regular silver polygons on the surface, such Ag_{50} cluster doesn't exhibit any geometrical polyhedron feature. The Ag_{50} shell was further consolidated by rich Ag···Ag interactions falling in the range of 2.851(2)−3.431(2) Å.

This 50-nucleus cluster is also templated by a novel rod-like POM, formulated as $Mo_8O_{28}^{8-}$, which can be seen as three Mo_4O_4 cubanes fused together by sharing two Mo_2O_2 rhombus faces (Fig. 3c), or described to eight edge-shared MoO_6 octahedra (Fig. 3d). The BVS[19] also verified + 6 oxidation state of eight Mo atoms (Mo1-Mo8: 5.865, 5.431, 5.648, 5.889, 5.868, 5.748, 6.092, and 5.738). The surface of $Mo_8O_{28}^{8-}$ has 20 terminal, 4 μ_2 bridging and 4 μ_4 bridging O atoms. Among these O atoms, only 20 terminal O atoms participate to the coordination with Ag atoms (Supplementary Fig. 4). Compared to the starting material α-$Mo_8O_{26}^{4-}$, $Mo_8O_{28}^{8-}$ has higher negative charges and more O atoms, which endow it as a better template in the assembly of silver clusters. The $Mo_8O_{28}^{8-}$ in **SD/Ag50**, to the best of our knowledge, has never been reported in POM-templated silver clusters and classic POM chemistry.

Inspired by the above discussed structure features of **SD/Ag44**, both $PhCOO^-$ ligands and weakly coordinated CH_3CN molecules are the potential reaction active sites, and the POM template can be also varied depending on the solution acidity. In fact, we found the transformation of **SD/Ag44** to **SD/Ag50** can facilely work by adding additional PhCOOH without changing any other reaction conditions. Based on the comparisons of their structures, such cluster-to-cluster structural transformation is a rare occurrence that simultaneously involved inner anion template ($Mo_6O_{22}^{8-} \rightarrow Mo_8O_{28}^{8-}$) and outer silver shell ($Ag_{44} \rightarrow Ag_{50}$). In this transformation process, the degree of condensation of molybdate was increased, resulting in the growth of $Mo_6O_{22}^{8-}$ to $Mo_8O_{28}^{8-}$. The larger POM template thus enlarges the outer silver shell from Ag_{44} to Ag_{50}. We also tried to synthesize **SD/ Ag50** without the transformation step by directly adding more PhCOOH into the reaction system, however, the **SD/Ag50** can be only isolated with a quite low yield (< 5%), whereas using the transformation synthesis route, it can reach up to more than 50%. Thus, PhCOOH-induced structural transformation might provide a new method for the high-yield synthesis of some silver clusters that are otherwise difficult to access. Moreover, this transformation reaction should be a thermodynamics controlled reaction, so **SD/Ag50** should be more stable than **SD/Ag44**.

Fig. 3 Single-crystal X-ray structure of **SD/Ag50**. **a** Molecular structure of **SD/Ag50** trapping a $Mo_8O_{28}^{8-}$ anion as template (Color legend: Ag: purple; S: yellow; Mo: green; O: red; C: gray; N: blue). **b** The ball-and-stick mode of $Ag_{50}S_{24}$ shell. The ball-and-stick (**c**) and polyhedral (**d**) modes showing the inner $Mo_8O_{28}^{8-}$ anion

ESI-MS of SD/Ag44 and SD/Ag50. In order to investigate solution behaviors of both clusters, the ESI-MS of **SD/Ag44** and **SD/Ag50** dissolved in dichloromethane were measured in the positive ion mode. As shown in Fig. 4a, there are a series of +2 species (**1a**-**1k**) centered at the m/z range of 2000–8000. The most dominant peak centered at 4392.48 (**1e**) was assigned to [Δ ($^iPrS)_{26}(PhCOO)_8(CH_2Cl_2)_2(H_2O)]^{2+}$ based on the superimposable observed and simulated isotope patterns (Cal. 4392.49; Δ = $Mo_6O_{22}@Ag_{44}$ hereafter). Similar formula assignment for each labeled species in ESI-MS was also performed as listed in Supplementary Table 4. Based on the assigned formula, we found the core of **SD/Ag44** is quite stable just with some surface ligand exchange between $PhCOO^-$ and $^iPrS^-$ such as those observed in paired species of **1b** and **1c**, **1 g** and **1 h**, and **1j** and **1k**. The 11 identified species existed in the solution, suggesting a typical coordination-disassociation equilibrium state, which may be broken by introducing some exotic stimuli, then producing some new species.
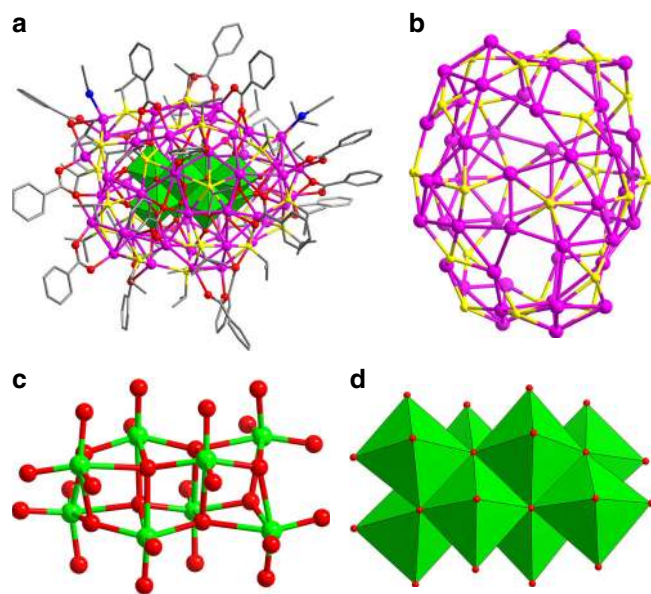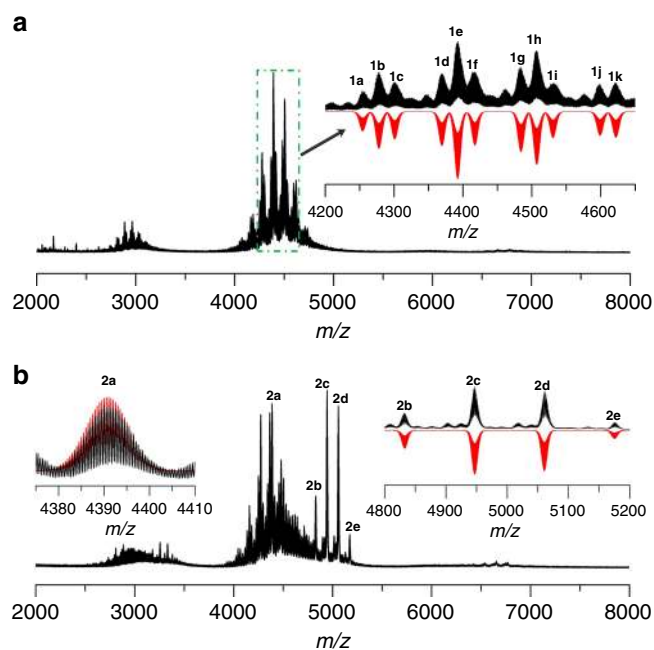
a

b

Fig. 4 ESI-MS. **a** Positive ion mode ESI-MS of the crystals of **SD/Ag44** dissolved in dichloromethane. Inset: The zoom-in mass spectrum of experimental (black line) and simulated (red line) isotope patterns for each labeled species. **b** Positive ion mode ESI-MS of the crystals of **SD/Ag50** dissolved in dichloromethane. Insets: The zoom-in mass spectrum of experimental (black lines) and simulated (red lines) isotope patterns for each labeled species

More complicated ESI-MS was observed for **SD/Ag50** in its dichloromethane solution (Fig. 4b). Carefully analyzing the isotope distribution of the observed peaks in the m/z range of 2000–8000, we found all these peaks were bivalent species with a parent ion peak of **SD/Ag50** detected at the m/z 5175.19 (**2e**), corresponding to $[Mo_8O_{28}@Ag_{50}(^iPrS)_{24}(PhCOO)_{16}]^{2+}$ (Cal. 5175.23), which can be formed by losing all the acetonitrile molecules and two $PhCOO^-$ ligands from **SD/Ag50**. The neighbor peak centered at m/z 5060.72 (**2d**) can be assigned to $[Mo_8O_{28}@Ag_{49}(^iPrS)_{24}(PhCOO)_{15}]^{2+}$ (Cal. 5060.76), corresponding to loss one PhCOOAg from **2e**. The most dominant peak (**2c**) was observed at m/z 4947.25, assigned to $[Mo_8O_{28}@Ag_{47}(^iPrS)_{22}(PhCOO)_{15}(CH_2Cl_2)(H_2O)_3]^{2+}$ (Cal. 4947.32). The other identified species were shown in Supplementary Table 5. Of note, a series of peaks in the m/z range of 4200–4700 are quite similar to those in ESI-MS of **SD/Ag44**. For example, the peak (**2a**) centered at 4391.01 can be ascribed to $[\Delta(^iPrS)_{25}(PhCOO)_9(CH_2Cl_2)(H_2O)_3]^{2+}$ (Cal. 4391.03). These results demonstrated (i) **SD/Ag50** can maintain its integrity in dichloromethane, and (ii) **SD/Ag50** can partially decompose to the closely related species to **SD/Ag44**.

Transformation mechanism study. How the transformation process happened and proceeded are intriguing issues in this system. To gain further insights into the transformation mechanism, we carried out a series of specific experiments including pH values measurements, comparable synthesis, and solution species tracking by ESI-MS during the transformation.

After synthesis of **SD/Ag44**, the pH of mother liquor is 10.45, then decreases to 8.20 upon adding PhCOOH, which is favorable to the further condensation reaction of molybdates[28]. To rule out

the $Mo_8O_{28}^{8-}$ being transformed from the residual molybdate species in mother liquor, we also used fresh crystals of **SD/Ag44** and clean CH_3CN as solvent to do the transformation reaction and **SD/Ag50** can also be formed, which suggested the $Mo_8O_{28}^{8-}$ must be transformed from the interior $Mo_6O_{22}^{8-}$ in **SD/Ag44**. Meanwhile, this result also unambiguously indicated that the smaller-to-larger silver nanocluster conversion from **SD/Ag44** to **SD/Ag50** genuinely started from **SD/Ag44** instead of other silver precursors.

As we know, ESI-MS is a promising analytical tool that provides considerable speciation information in solution[29–32]. Cronin group have contributed largely to this field by using ESI-MS to detect new POM species and track transformation of POMs[33–35]. This technique was also profoundly used by Xie group to study growth mechanism of gold nanoclusters or reactivity[36–40]. However, using ESI-MS to study transformation or reactivity of silver clusters has remained a black box to date. To shed light on the details of transformation process from Ag_{44} to Ag_{50}, we tracked the solution species evolution over the course of 240 min upon addition of PhCOOH (0.32 mmol, 39.1 mg) in the CH_2Cl_2 solution of Ag_{44} cluster by time-dependent ESI-MS. In order to guarantee comparable intensity of signals for each species at different times, a generalized operation for the sampling and analysis was established and uniform instrument parameters were maintained. At scheduled time intervals, 500 μL aliquots of the reaction solution were extracted, and immediately infused (240 μL/h) to the mass spectroscopy without dilution for subsequent measurement. To set the baseline and finishing line for this monitoring process, we also incorporated the ESI-MS spectra of Ag_{44} (black line) and Ag_{50} (dark green line) in CH_2Cl_2 into Fig. 5, respectively, although in-source fragmentation of them under our chosen ESI source parameters have been studied in above section. All formulae of labeled species in the ESI-MS in this section are listed in Supplementary Table 6 and hereafter only inner core compositions are shown below for clarity. Zoom-in ESI-MS including the simulated isotope distributions of all these species are shown in Supplementary Fig. 5. As depicted in Fig. 5a (0 min), once adding PhCOOH, four doubly charged species **1l**-**1o** appeared in the lower m/z range of 3600–4200 which are absent in original ESI-MS of Ag_{44} solution. The assigned formulae for **1l**-**1o** are $[Mo_5O_{18}@Ag_{38}]$ (**1l**), $[Mo_5O_{18}@Ag_{39}]$ (**1m**), and $[Mo_5O_{18}@Ag_{40}]$ (**1n and 1o**). In the higher m/z range of 4600–5300, the other five larger divalent species (**1p, 1q, 1r, 2d, and 2e**) are observed and can be assigned to $[Mo_8O_{28}@Ag_{45}]$ (**1p**), $[Mo_8O_{28}@Ag_{46}]$ (**1q**), $[Mo_8O_{28}@Ag_{47}]$ (**1r**), $[Mo_8O_{28}@Ag_{49}]$ (**2d**), and $[Mo_8O_{28}@Ag_{50}]$ (**2e**). Of note, the **2e** species is the parent ion of **SD/Ag50**. All these intermediates are smaller or larger than original Ag_{44} cluster and their formations are intensely dependent on the addition of PhCOOH.

The evolutions of species were further represented by the plots of signal intensity vs. time as shown in Fig. 5b. Upon adding PhCOOH, we observed four species (**1l**-**1o**) smaller than Ag_{44}, indicating the breakage of Ag_{44} shell was initiated by PhCOOH. As time going on (5–240 mins), the signal intensities of $[Mo_5O_{18}@Ag_{38}]$ (**1l**), $[Mo_5O_{18}@Ag_{39}]$ (**1m**), and $[Mo_5O_{18}@Ag_{40}]$ (**1n and 1o**) gradually decrease, whereas those of $[Mo_8O_{28}@Ag_{49}]$ (**2d**) and $[Mo_8O_{28}@Ag_{50}]$ (**2e**) become more intense, which suggested that the formation of Ag_{50} cluster is at the expense of smaller intermediate species such as **1l**-**1o** at this stage. Moreover, we also noted the POM template encapsulated in silver shell undergo a condensation reaction from $Mo_6O_{22}^{8-}$ to $Mo_8O_{28}^{8-}$ and the excess oxygen coordination sites permit for the linkage of more silver atoms, thus forming the cluster larger than Ag_{44}.

Based on above observations, we speculated that the outer silver shell was attacked and partially broken by PhCOOH during
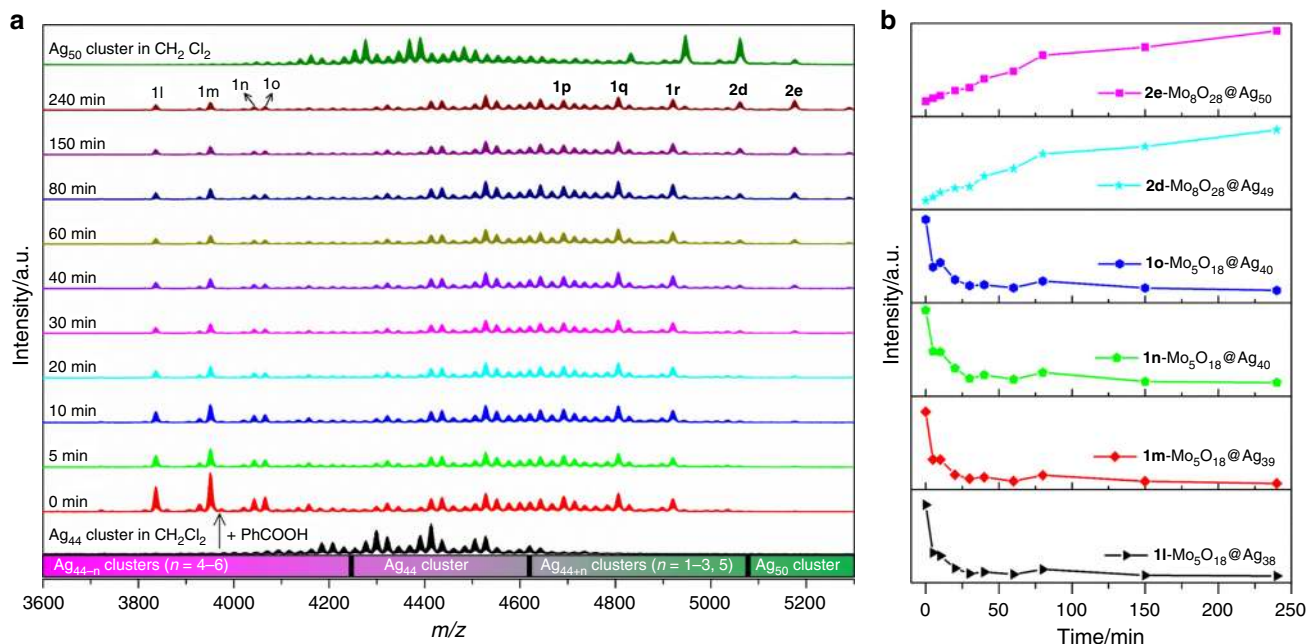
Fig. 5 Time-course ESI-MS. **a** Time-course ESI-MS of transformation from Ag_{44} to Ag_{50} cluster induced by adding PhCOOH. The detailed formulae of labeled species are listed in Supplementary Table 6. **b** Plots of ESI-MS peak intensity of selected intermediate species vs time during the transformation process

the initial stage, which resulted in the breakage of Ag_{44} shell in some extent, followed by the growth of inner $Mo_6O_{22}^{8-}$ anion to $Mo_8O_{28}^{8-}$. Due to the addition of PhCOOH, the solution becomes more acidity, thus larger $Mo_8O_{28}^{8-}$ was formed via condensation reaction. The decomposed fragments further reassemble around the new template to form final large Ag_{50} cluster. Finally, the overall breakage-growth-reassembly (BGR) mechanism was established for this transformation process (Fig. 6).

Universality of acid-induced transformation. We also introduced different substituted benzoic acids such as 4-methylbenzoic acid (4-MePhCOOH) and 3-methylbenzoic acid (3-MePhCOOH) into above transformation process (Supplementary Fig. 1) to check the universality of transformation. Of note, the similar Ag_{50} clusters can be also isolated after acid induction and characterized by SCXRD analysis, which showed their structures are quite similar with inner $Mo_8O_{28}^{8-}$ and outer Ag_{50} shell but just with different substituted degree of benzoates on the surface. The details of molecular structures and crystallography tables were shown in Supplementary Figs. 6–8 and Supplementary Table 1, respectively. Their formulae were determined as $[Mo_8O_{28}@Ag_{50}(^iPrS)_{24}(4\text{-MePhCOO})_{14}(PhCOO)_4(CH_3CN)_4]$ (**SD/Ag50a**), $[Mo_8O_{28}@Ag_{50}(^iPrS)_{24}(4\text{-MePhCOO})_{16.5}(PhCOO)_{1.5}]$ (**SD/Ag50b**), and $[Mo_8O_{28}@Ag_{50}(^iPrS)_{24}(3\text{-MePhCOO})_{18}(3\text{-MePhCOOH})(CH_3CN)_2]$ (**SD/Ag50c**). The degree of substitution reaction between substituted benzoates and $PhCOO^-$ is intensely depended on the dose of substituted benzoates. For example, when increasing amount of 4-MePhCOOH from 0.3 to 0.6 mmol, the **SD/Ag50b** can be formed instead of **SD/Ag50a**. These results not only justified a universal acid-induced transformation fashion to synthesize larger sized silver clusters but also may bring new functionalities for silver clusters by ligand exchanges.

UV-Vis absorption spectra and luminescence properties. The solid state UV/Vis absorption spectra of **SD/Ag44**, **SD/Ag50**, and
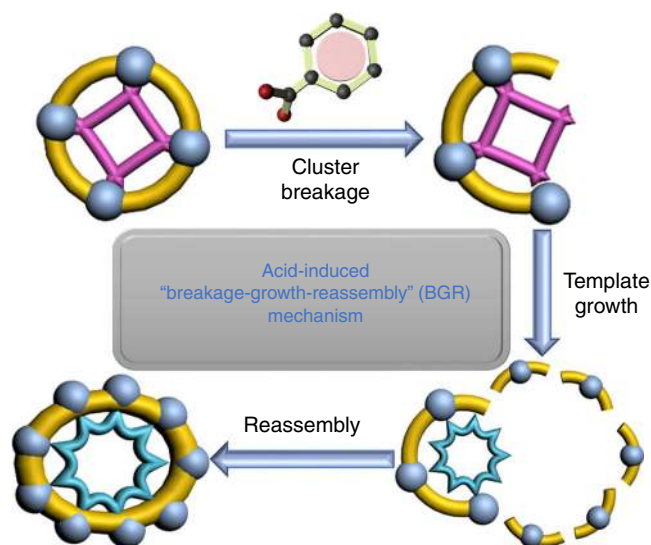

Fig. 6 The proposed breakage-growth-reassembly mechanism for the transformation process from **SD/Ag44** to **SD/Ag50**

$(^iPrSAg)_n$ precursor were measured at room temperature. As shown in Supplementary Fig. 19, **SD/Ag44** and **SD/Ag50** exhibit one intense absorption centered at 344 and 356 nm in the UV region. The UV absorption peaks can be attributed to the $n \rightarrow \pi^*$ transition of $^iPrS^-$, as similar observed in the spectrum of the precursor $(^iPrSAg)_n$. The HOMO–LUMO gaps were determined as 2.35, 2.33, and 2.52 eV for **SD/Ag44**, **SD/Ag50**, and $(^iPrSAg)_n$ precursor by using the transformed Kubelka–Munk plots, respectively (Supplementary Fig. 20), which are consistent with their yellow appearances.

We also checked the emission behaviors of **SD/Ag44** and **SD/Ag50** at both 298 and 77 K using hand-held UV light
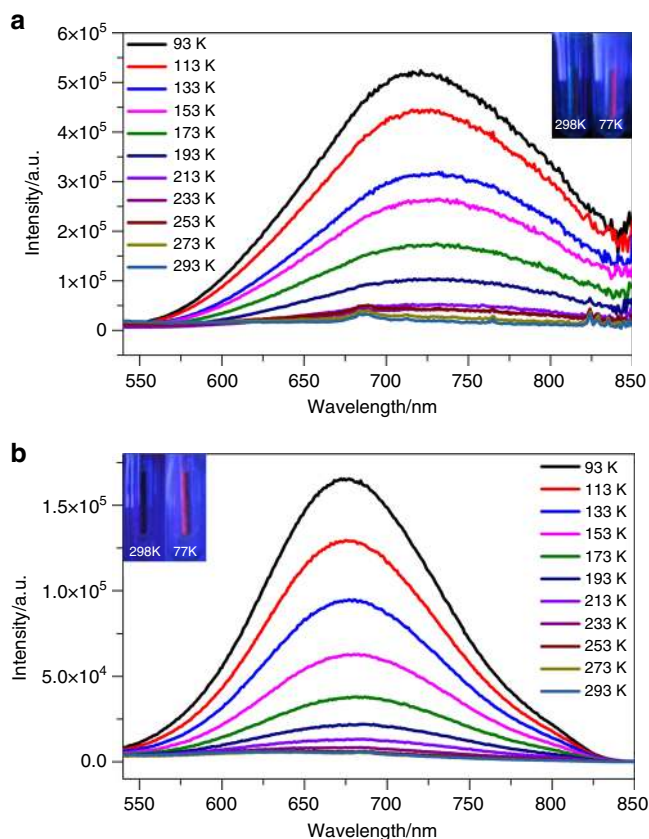
Fig. 7 Luminescence properties of **SD/Ag44** and **SD/Ag50**. Varied-temperature emission spectra of **SD/Ag44** (**a**) and **SD/Ag50** (**b**) in solid state under the excitation of 463 nm, Insets: the photographs of **SD/Ag44** and **SD/Ag50** irradiated by hand-held UV light ($\lambda_{ex} = 365$ nm) at 298 and 77 K

($\lambda_{ex} = 365$ nm). Preliminarily, both **SD/Ag44** and **SD/Ag50** emit red luminescence at 77 K but become emission-silent at 298 K. The on-off phenomena of them are reversible between 298 and 77 K and can be directly observed by naked eyes (See the insets in Fig. 7). For detailed studies of such observations, varied-temperature luminescent spectra of **SD/Ag44** and **SD/Ag50** were measured from 93 to 293 K in the solid state. As shown in Fig. 7a, **SD/Ag44** emits near-infrared (NIR) light ($\lambda_{em} = 719$ nm) at 93 K and is almost non-emissive from 213–293 K. The maximum emission peak gradually red-shifts to 725 nm upon warming to 193 K along with obvious decrease of emission intensity. For **SD/Ag50**, its maximum emission peak red-shifts from 674 nm at 93 K to 686 nm at 233 K with gradually decayed emission intensity, after which no obvious emissions can be detected above 253 K. These NIR emissions at cryogenic temperature can be similarly attributed to the ligand-to-metal charge transfer (LMCT, charge transfer from S 3p to Ag 5 s) perturbed by Ag···Ag interaction[41,42]. The temperature-dependent emissions should be in the connection with the variations of molecule rigidity and argentophilicity under different temperatures[43,44]. The emission lifetimes of both **SD/Ag44** and **SD/Ag50** at 93 K fall in the microsecond scale (Supplementary Fig. 21), suggesting the phosphorescent triplet excitation state[45]. It is worth to noting that the emission intensities have good linearity correlation with respect to temperature in the low temperature regions (Supplementary Fig. 22). The linearity equations can be described as $I_{max} = -3977T + 876273$ (correlation coefficient = 0.985) and

$I_{max} = -1461T + 294270$ (correlation coefficient = 0.979) for **SD/Ag44** (93–213 K) and **SD/Ag50** (93–193 K), respectively.

Discussion

In conclusion, we synthesized and characterized two thiolate/benzoate co-protected Ag$_{44}$ and Ag$_{50}$ clusters. The latter can be facilely synthesized by PhCOOH-induced transformation reaction, resulting in the enlargement of both inner anion template ($Mo_6O_{22}^{8-} \rightarrow Mo_8O_{28}^{8-}$) and outer silver shell (Ag$_{44} \rightarrow$ Ag$_{50}$). The solution behaviors of Ag$_{44}$ and Ag$_{50}$ clusters were studied in details using ESI-MS technique. The overall breakage-growth-reassembly (BGR) transformation mechanism was also established based on the time-dependent ESI-MS, which revealed several small fragmented species ([Mo$_5$O$_{18}$@Ag$_{38}$]~ [Mo$_5$O$_{18}$@Ag$_{40}$]) and large intermediates ([Mo$_8$O$_{28}$@Ag$_{45}$]~ [Mo$_8$O$_{28}$@Ag$_{49}$]), as well as their abundance evolutions along with reaction going on. To our knowledge, this is the first example of the transformation of a smaller silver cluster into a larger one via anion template growth. This work not only revealed the important reactivity of silver clusters with acids but also provide a novel method for synthesizing larger silver clusters that are otherwise difficult to obtain.

Methods

Synthesis of (^{i}PrSAg)$_n$. (^{i}PrSAg)$_n$ was prepared by the following reported procedure[43]. The solution of AgNO$_3$ (30 mmol, 5.1 g) in 75 mL acetonitrile was mixed with 100 mL ethanol containing ^{i}PrSH (30 mmol, 2.8 mL) and 5 mL Et$_3$N under stirring for 3 h in the dark at room temperature, then the yellow powder of (^{i}PrSAg)$_n$ was isolated by filtration and washed with 10 mL ethanol and 20 mL ether, then dried in the ambient environment (yield: 97 %, based on AgNO$_3$).

Synthesis of SD/Ag44. Typically, the mixture of PhCOOAg (0.1 mmol, 22.9 mg), (^{i}PrSAg)$_n$ (0.05 mmol, 9.2 mg), and (^{n}Bu$_4$N)$_4$(α-Mo$_8$O$_{26}$) (0.0002 mmol, 4.2 mg) were dissolved in 5 mL acetonitrile then sealed into 25 mL Teflon-lined autoclave and heated at 65 °C under autogenous pressure for 2000 min. After cooling to room temperature, yellow crystals were isolated with a yield of 45 % (based on (^{i}PrSAg)$_n$). Elemental analyses calc. (found) for **SD/Ag44** (C$_{180}$H$_{232}$Ag$_{44}$Mo$_6$N$_4$O$_{54}$S$_{20}$): C, 23.30 (23.18); H, 2.52 (2.47); N 0.60 (0.55) %. Selected IR peaks (cm^{-1}): 3682 (w), 2961 (m), 1589 (w), 1523 (m), 1454 (w), 1371 (s), 1241 (w), 1149 (w), 1032 (s), 1014 (m), 811 (w), 715 (m), 675 (m), 588 (w).

Synthesis of SD/Ag50. Another portion of PhCOOH (0.32 mmol, 39.1 mg) was added into the mother liquor after the synthesis of **SD/Ag44** but without removing crystals of **SD/Ag44**, then this mixture was again sealed into 25 mL Teflon-lined autoclave and heated at 65 °C under autogenous pressure for 2000 min. After cooling to room temperature, yellow crystals were isolated with a yield of 50% (based on (^{i}PrSAg)$_n$). Elemental analyses calc. (found) for **SD/Ag50** (C$_{210}$H$_{276}$Ag$_{50}$Mo$_8$N$_6$O$_{64}$S$_{24}$): C, 23.09 (23.18); H, 2.57 (2.48); N 0.78 (0.70) %. Selected IR peaks (cm^{-1}): 2955 (w), 2907 (w), 1589 (w), 1528 (s), 1454 (w), 1371 (s), 1241 (m), 1144 (w), 1046 (m), 910 (w), 880 (m), 830 (m), 800 (m), 714 (s), 671 (m), 635 (m), 610 (m).

Synthesis of SD/Ag50a. The synthesis conditions were similar to those described for **SD/Ag50** except using 4-MePhCOOH (0.33 mmol, 44.9 mg) instead, yellow crystals were isolated with a yield of 36 % (based on (^{i}PrSAg)$_n$). Elemental analyses calc. (found) for **SD/Ag50a** (C$_{220}$H$_{298}$Ag$_{50}$Mo$_8$N$_4$O$_{64}$S$_{24}$): C, 24.12 (23.97); H, 2.74 (2.58); N 0.51 (0.46) %. Selected IR peaks (cm^{-1}): 3670 (w), 2949 (w), 2912 (w), 1584 (w), 1520 (m), 1453 (w), 1368 (s), 1242 (m), 1169 (m), 1148 (m), 1052 (m), 916 (m), 878 (m), 831 (m), 796 (s), 759 (s), 712 (m), 632 (s), 606 (s).

Synthesis of SD/Ag50b. The synthesis conditions were similar to those described for **SD/Ag50** except using 4-MePhCOOH (0.57 mmol, 77.6 mg) instead, yellow crystals were isolated with a yield of 30 % (based on (^{i}PrSAg)$_n$). Elemental analyses calc. (found) for **SD/Ag50b** (C$_{214.5}$H$_{291}$Ag$_{50}$Mo$_8$O$_{64}$S$_{24}$): C, 23.80 (23.59); H, 2.71 (2.58) %. Selected IR peaks (cm^{-1}): 3674 (w), 2971 (w), 2905 (w), 1584 (w), 1524 (m), 1453 (w), 1368 (s), 1237 (m), 1173 (w), 1149 (w), 1047 (s), 911 (m), 877 (s), 834 (m), 798 (m), 763 (s), 712 (m), 632 (s), 605 (s).

Synthesis of SD/Ag50c. The synthesis conditions were similar to those described for **SD/Ag50** except using 3-MePhCOOH (0.57 mmol, 77.6 mg), yellow crystals were isolated with a yield of 33 % (based on (^{i}PrSAg)$_n$). Elemental analyses calc. (found) for **SD/Ag50c** (C$_{234}$H$_{317}$Ag$_{50}$Mo$_8$N$_5$O$_{66}$S$_{24}$): C, 25.12 (24.98); H, 2.86

(2.74); N 0.63 (0.57) %. Selected IR peaks (cm^{-1}): 3673 (w), 2955 (w), 2912 (w), 1592 (w), 1528 (m), 1450 (w), 1368 (s), 1236 (m), 1149 (m), 1078 (m), 1049 (m), 914 (m), 875 (m), 780 (s), 714 (m), 671 (s), 631 (s), 601 (s).

Data availability

References

1. Young, A. G. & Hanton, L. R. Square planar silver(I) complexes: a rare but increasingly observed stereochemistry for silver(I). *Coord. Chem. Rev.* **252**, 1346–1386 (2008).
2. Schmidbaur, H. & Schier, A. Argentophilic interactions. *Angew. Chem. Int. Ed. Engl.* **54**, 746–784 (2015).
3. Liu, J.-W. et al. Anisotropic assembly of Ag_{52} and Ag_{76} nanoclusters. *J. Am. Chem. Soc.* **140**, 1600–1603 (2018).
4. Corrigan, J. F., Fuhr, O. & Fenske, D. Metal chalcogenide clusters on the border between molecules and materials. *Adv. Mater.* **21**, 1867–1871 (2009).
5. Xie, Y.-P., Jin, J.-L., Duan, G.-X., Lu, X. & Mak, T. C. W. High-nuclearity silver (I) chalcogenide clusters: a novel class of supramolecular assembly. *Coord. Chem. Rev.* **331**, 54–72 (2017).
6. Jin, R. C., Zeng, C. J., Zhou, M. & Chen, Y. X. Atomically precise colloidal metal nanoclusters and nanoparticles: fundamentals and opportunities. *Chem. Rev.* **116**, 10346–10413 (2016).
7. Rais, D. et al. Anion-templated syntheses of rhombohedral silver-alkynyl cage compounds. *Angew. Chem. Int. Ed. Engl.* **40**, 3464–3467 (2001).
8. Li, X.-Y. et al. A platonic solid templating Archimedean solid: an unprecedented nanometre-sized Ag_{37} cluster. *Nanoscale* **7**, 8284–8288 (2015).
9. Wang, Q.-M., Lin, Y.-M. & Liu, K.-G. Role of anions associated with the formation and properties of silver clusters. *Acc. Chem. Res.* **48**, 1570–1579 (2015).
10. Li, S. et al. Atom-precise modification of silver(I) thiolate cluster by shell ligand substitution: a new approach to generation of cluster functionality and chirality. *J. Am. Chem. Soc.* **140**, 594–597 (2018).
11. Anson, C. E. et al. Synthesis and crystal structures of the ligand-stabilized over chalcogenide clusters $[Ag_{154}Se_{77}(dppxy)_{18}]$, $[Ag_{320}(StBu)_{60}S_{130}(dppp)_{12}]$, $[Ag_{352}S_{128}(StC_5H_{11})_{96}]$, and $[Ag_{490}S_{188}(StC_5H_{11})_{114}]$. *Angew. Chem. Int. Ed. Engl.* **47**, 1326–1331 (2008).
12. Wang, Z. et al. Assembly of silver trigons into a buckyball-like Ag_{180} nanocage. *Proc. Natl Acad. Sci. USA* **114**, 12132–12137 (2017).
13. Hau, S. C. K., Cheng, P.-S. & Mak, T. C. W. Enlargement of globular silver alkynide cluster via core transformation. *J. Am. Chem. Soc.* **134**, 2922–2925 (2012).
14. Liu, H. et al. Acid-base-triggered structural transformation of a polyoxometalate core inside a dodecahedrane-like silver thiolate shell. *Angew. Chem. Int. Ed. Engl.* **55**, 3699–3703 (2016).
15. Parr, R. G. & Pearson, R. G. Absolute hardness-companion parameter to absolute electronegativity. *J. Am. Chem. Soc.* **105**, 7512–7516 (1983).
16. Chalmers, R. A. & Sinclair, A. G. Organic molybdate complexes. *J. Inorg. Nucl. Chem.* **29**, 2065–2080 (1967).
17. Huang, R.-W. et al. Hypersensitive dual-function luminescence switching of a silver-chalcogenolate cluster-based metal-organic framework. *Nat. Chem.* **9**, 689–697 (2017).
18. Dhayal, R. S. et al. $[Ag_{21}\{S_2P(O^iPr)_2\}_{12}]^+$: an eight-electron superatom. *Angew. Chem. Int. Ed. Engl.* **54**, 3702–3706 (2015).
19. Brown, I. D. & Altermatt, D. Bond-valence parameters obtained from a systematic analysis of the inorganic crystal-structure database. *Acta Crystallogr. B* **41**, 244–247 (1985).
20. Li, Y.-W. et al. Two unprecedented POM-based inorganic organic hybrids with concomitant heteropolytungstate and molybdate. *Inorg. Chem.* **56**, 2481–2489 (2017).
21. Li, X.-Y. et al. Atom-precise polyoxometalate-Ag_2S core-shell nanoparticles. *Chem.-Asian J.* **10**, 1295–1298 (2015).
22. Li, X.-Y. et al. Anion-templated nanosized silver clusters protected by mixed thiolate and diphosphine. *Nanoscale* **9**, 3601–3608 (2017).
23. Qiao, J., Shi, K. & Wang, Q.-M. A giant silver alkynyl cage with sixty silver(I) ions clustered around polyoxometalate templates. *Angew. Chem., Int. Ed.* **49**, 1765–1767 (2010).
24. Gao, G.-G., Cheng, P.-S. & Mak, T. C. W. Acid-induced surface functionalization of polyoxometalate by enclosure in a polyhedral silver-alkynyl cage. *J. Am. Chem. Soc.* **131**, 18257–18259 (2009).
25. Su, Z.-H., Zhou, B.-B., Zhao, Z.-F. & Zhang, X. A novel 1D chain compound constructed from copper-complex fragments-substituted dilacunary beta-octamolybdate units and saturated beta-octamolybdate clusters. *Inorg. Chem. Commun.* **11**, 334–337 (2008).
26. Wang, J.-P., Du, X.-D. & Niu, J.-Y. A novel 1D organic-inorganic hybrid based on alternating heteropolyanions $[GeMo_{12}O_{40}]^{4-}$ and isopolyanions $[Mo_6O_{22}]^{8-}$. *J. Solid. State Chem.* **179**, 3260–3264 (2006).
27. Dai, L., Wang, E., You, W. & Zhang, Z. Synthesis and electrochemical properties of a new 1D organic-inorganic hybrid compound based on Keggin-type heteropolyanions and isopolyanions decorated by transition metal fragments. *J. Clust. Sci.* **19**, 511–519 (2008).
28. Cruywagen, J. J. Protonation, oligomerization, and condensation reactions of vanadate(V), molybdate(VI), and tungstate(VI). *Adv. Inorg. Chem.* **49**, 127–182 (2000).
29. Hu, Y.-Q. et al. Tracking the formation of a polynuclear Co_{16} complex and its elimination and substitution reactions by mass spectroscopy and crystallography. *J. Am. Chem. Soc.* **135**, 7901–7908 (2013).
30. Newton, G. N., Cooper, G. J. T., Koegerler, P., Long, D.-L. & Cronin, L. Trading templates: supramolecular transformations between $\{Co^{II}_{13}\}$ and $\{Co^{II}_{12}\}$ nanoclusters. *J. Am. Chem. Soc.* **130**, 790–791 (2008).
31. Deng, Y.-K. et al. Hierarchical assembly of a $\{Mn^{II}_{15}Mn^{III}_4\}$ brucite disc: step-by-step formation and ferrimagnetism. *J. Am. Chem. Soc.* **138**, 1328–1334 (2016).
32. Guo, L.-Y. et al. Core-shell $\{Mn_7 \subset (Mn,Cd)_{12}\}$ assembled from core $\{Mn_7\}$ disc. *J. Am. Chem. Soc.* **139**, 14033–14036 (2017).
33. Surman, A. J. et al. Sizing and discovery of nanosized polyoxometalate clusters by mass spectrometry. *J. Am. Chem. Soc.* **138**, 3824–3830 (2016).
34. Cameron, J. M. et al. Investigating the transformations of polyoxoanions using mass spectrometry and molecular dynamics. *J. Am. Chem. Soc.* **138**, 8765–8773 (2016).
35. Miras, H. N. et al. Oscillatory template exchange in polyoxometalate capsules: a ligand-triggered, redox-powered, chemically damped oscillation. *J. Am. Chem. Soc.* **134**, 6980–6983 (2012).
36. Yuan, X. et al. Balancing the rate of cluster growth and etching for gram-scale synthesis of thiolate-protected Au_{25} nanoclusters with atomic precision. *Angew. Chem. Int. Ed. Engl.* **53**, 4623–4627 (2014).
37. Luo, Z. et al. Toward understanding the growth mechanism: tracing all stable intermediate species from reduction of Au(I)-thiolate complexes to evolution of Au_{25} nanoclusters. *J. Am. Chem. Soc.* **136**, 10577–10580 (2014).
38. Yao, Q. et al. Precise control of alloying sites of bimetallic nanoclusters via surface motif exchange reaction. *Nat. Commun.* **8**, 1555 (2017).
39. Yao, Q. et al. Understanding seed-mediated growth of gold nanoclusters at molecular level. *Nat. Commun.* **8**, 927 (2017).
40. Yao, Q. et al. Revealing isoelectronic size conversion dynamics of metal nanoclusters by a noncrystallization approach. *Nat. Commun.* **9**, 1979 (2018).
41. Yam, V. W.-W., Au, V. K.-M. & Leung, S. Y.-L. Light-emitting self-assembled materials based on d^8 and d^{10} transition metal complexes. *Chem. Rev.* **115**, 7589–7728 (2015).
42. Barbieri, A., Accorsi, G. & Armaroli, N. Luminescent complexes beyond the platinum group: the d^{10} avenue. *Chem Commun.* **0**, 2185–2193 (2008).
43. Wang, Z. et al. Johnson solids: anion-templated silver thiolate clusters capped by sulfonate. *Chemistry* **24**, 1640–1650 (2018).
44. Huang, R.-W. et al. Tandem silver cluster isomerism and mixed linkers to modulate the photoluminescence of cluster-assembled materials. *Angew. Chem. Int. Ed. Engl.* **57**, 8560–8566 (2018).
45. Wang, Z.-Y. et al. Atomically precise site-specific tailoring and directional assembly of superatomic silver nanoclusters. *J. Am. Chem. Soc.* **140**, 1069–1076 (2018).

Author contributions

Original idea was conceived by D.S., experiments and data analyses were performed by Z.W. and D.S., ESI-MS data were collected by H.-F.S., structure characterization was

performed by Z.W. and D.S., manuscript was drafted by D.S., Z.W., C.-H.T. and L.-S.Z. All authors have given approval to the manuscript.

Additional information

Supplementary Information accompanies this paper at https://doi.org/10.1038/s41467-018-06755-4.

Competing interests: The authors declare no competing interests.

Reprints and permission information is available online at http://npg.nature.com/reprintsandpermissions/

Publisher's note: Springer Nature remains neutral with regard to jurisdictional claims in published maps and institutional affiliations.